

Contents lists available at [ScienceDirect](https://www.sciencedirect.com)

Remote Sensing of Environment

journal homepage: www.elsevier.com/locate/rse

Anthropogenic marine debris over beaches: Spectral characterization for remote sensing applications



Tomás Acuña-Ruz^a, Diego Uribe^a, Richard Taylor^a, Lucas Amézquita^a, María Cristina Guzmán^a, Javier Merrill^c, Paula Martínez^b, Leandro Voisin^b, Cristian Mattar B.^{a,*}

^a *Laboratory for Analysis of the Biosphere (LAB), University of Chile, Chile.*

^b *Advanced Mining Technology Center (AMTC), University of Chile, Chile.*

^c *CSIRO Chile International Centre of Excellence, Chile.*

ARTICLE INFO

Keywords:

Anthropogenic marine debris (AMD)

Hyperspectral characterization

High spatial resolution

Support vector machine

Chiloé

Chile

ABSTRACT

Anthropogenic Marine Debris (AMD) is one of the most important pollutants in the oceans. Millions of tons of debris across oceans have created a critical environmental problem. This study presents a novel method aimed to improve the identification of macroplastics through remote sensing over beaches, combining AMD hyperspectral laboratory characterization and digital supervised classification in high spatial resolution imagery. Several samples were collected from the Chiloé Island beaches, Chile. Spectral signature samples and physical properties were assessed through laboratory work. HyLogger3[®] (CSIRO), PS-300 Apogee and ASD Field Spec hyperspectral systems were used to characterize each sample. Using those measurements, a spectral library was generated by processing, filtering and sorting the spectral data gathered, determining distinctive spectral bands for digital classification. By using this spectral library, a digital classification method was implemented over World-View 3 imagery, covering the three beaches selected as test sites. Distinct classification methods and geospatial analyses were applied to determine land cover composition, aimed for the detection of Styrofoam and the rest of anthropogenic marine debris. Four field campaigns were carried out to validate the AMD classification and mass retrievals, performed on > 300 ground based points. The AMD hyperspectral library was successfully applied for an AMD digital classification in satellite imagery. Support Vector Machine method showed the best performance, resulting in an overall accuracy equivalent to 88% and over 50 tons of debris estimated on the pilot beaches. These results prove the feasibility of quantifying macro-AMD through the integration of hyperspectral laboratory measurements and remote sensing imagery, allowing to estimate anthropogenic influence on natural ecosystems and providing valuable information for further development of the methodology and sustainable AMD management.

1. Introduction

From the north to the south pole, anthropogenic marine debris (AMD) has accumulated on coastlines, in estuaries, marshes, ocean surfaces and even down into its depths (Thompson et al., 2009; Woodall et al., 2014). AMD represents a concern for many disciplines and communities (Bergmann et al., 2015; Nelms et al., 2017; UNEP, 2009). Studies on the composition of AMD in different regions of the world indicate that plastics represent between 50% and 90% of the total, which varies according to the proximity to the sources of pollution (Derraik, 2002; Galgani et al., 2010; Pham et al., 2014). Moreover, global plastic production soared from 5 million tons to 311 million tons between the years 1960 and 2014 (PlasticsEurope, 2012, 2015).

Some examples of how AMD impacts the environment and the fauna includes entanglement and ingestion, which can lead to the injury and/or death of turtles, cetaceans, seals, birds and fishes (Rochman and Browne, 2013; Gall and Thompson, 2015; Hardesty et al., 2015; Newman et al., 2015; Lavender, 2017; Nelms et al., 2017; Chubarenko and Stepanova, 2017; Unger et al., 2016). AMD can transport organic and non-organic pollutants across beaches and oceans (Barnes, 2002; Barnes and Milner, 2005; Nelms et al., 2017; Chubarenko and Stepanova, 2017; Romera-Castillo et al., 2018), on the seafloor it provides shelter for small animals and can reduce the gas exchange between the water column and the sediment, displacing multiple benthonic species (Watters et al., 2010; Lavender, 2017). It also impacts human communities with the loss of aesthetic value and the reduction

* Corresponding author at: Obispo Vielmo No. 62, Coyhaique, Chile.

E-mail address: cristian.mattar@uaysen.cl (C. Mattar B.).

<https://doi.org/10.1016/j.rse.2018.08.008>

Received 1 December 2017; Received in revised form 7 August 2018; Accepted 9 August 2018

Available online 27 August 2018

0034-4257/ © 2018 Elsevier Inc. All rights reserved.

of economic activities on beaches and other public locations (Cheshire et al., 2009). It is widely thought that AMD can be a major factor in the possible collapse of the ocean health, being a global stress together with others transformations, such as rising sea levels, warming waters, and changes in the ocean chemistry (Cheshire et al., 2009; ICC, 2009). However, the long-term impact of marine pollution on the deterioration of ecosystems and in the loss of biodiversity is still uncertain (Hyrenbach and Kennish, 2008; Mouat et al., 2009).

In Chile, numerous studies were carried out to identify, quantify and describe AMD on beaches and in coastal waters which have shown that anthropogenic marine debris is a problem along the entire coast (Bravo et al., 2009; Hidalgo-Ruz and Thiel, 2013; Hinojosa and Thiel, 2009; Hinojosa et al., 2011). Some of the studies highlight the abundance of plastics, either because they were found at all the points under study, or because they made up over 80% of the total observed AMD (Bourne and Clarke, 1984; Bravo et al., 2009; Hinojosa and Thiel, 2009; Ivar do Sul and Costa, 2007; Thiel et al., 2003). The abundance and composition of AMD found in southern Chile might be related to the aquaculture activity in the area (Hidalgo-Ruz and Thiel, 2013; Hinojosa and Thiel, 2009), which requires the use of plastics such as ropes, floats, and buoys. Eventually, part of the materials breaks off from the structures and can float away for long distances as floating marine debris (Astudillo et al., 2009; Jara and Jaramillo, 1979; Thiel et al., 2003). How far they travel depends on ocean currents and winds, as well as how long each object stays afloat, which is usually reduced by water saturation, biofouling, and stranding on beaches (Astudillo et al., 2009; Fujieda and Sasaki, 2005; Gregory and Andradý, 2003).

In Los Lagos region of Chile, rapid growth in aquaculture since the 1980s has had undesired side effects, such as beaches polluted with AMD, especially on the Island of Chiloé (Kießling et al., 2017). According to DIRECTEMAR reports (2016), 141.8 linear km of coastline on Chiloé's channels and fjords are affected by AMD, mainly in the form of polystyrene buoys (i.e. Styrofoam), plastic ropes, and remnants of nets or meshes used in aquaculture. The region is currently home to 39% of Chile's salmon production (*Salmo salar*, a foreign species to the marine ecosystem of Chiloé) and 99.9% of its mussel production (*Mytilus chilensis*), making it the region with the highest intensity and density of salmon and mussel farming in Chile (Hinojosa and Thiel, 2009; SERNAPESCA, 2015). This relates directly to the large quantities of AMD found in Chiloé, which vary between 10 and 50 Items/km² in the sea, and exceed the 200 Items/km² in areas such as the Desertores Islands (Hidalgo-Ruz and Thiel, 2013; Hinojosa and Thiel, 2009; Ivar do Sul and Costa, 2007).

Furthermore, due to the remoteness of the areas where AMD can potentially accumulate, such as uninhabited and geographically isolated islands, refined and widely applicable estimation methods must be developed (Convey et al., 2002; Morishige and McElwee, 2012). The methods for estimating AMD quantities and distribution can be grouped into the following categories: surveying on beaches, surveying from vessels, trawl sampling, surveying from diving, and surveying via satellite or aerial remote sensing (Brainard et al., 2000). To apply these, considerable logistics and economic resources are required, with remote sensing as the less constricted in spatial coverage and temporal resolution (Brainard et al., 2000; Driedger et al., 2015; McElwee et al., 2012; Pichel et al., 2012). However, remote sensing it is not widely developed for the detection of AMD in the marine environment (Driedger et al., 2015), and their identification through classification algorithm is still a challenge due to their variety and disposal in different site conditions and backgrounds (Morishige and McElwee, 2012).

Flow models may also be included in the previous categories, as a method that predicts distribution and quantities of AMD, considering the influence of oceanic flows in the trajectory and accumulation through simulation algorithms (Derraik, 2002; Sepulveda et al., 2011).

In remote sensing one of the primary detection methods are supervised classifications, which has multiple applications including the determination of environmental damage, monitoring land use, urban

planning, and tree species distribution (Michez et al., 2016; Zhong and Zhang, 2012). It has also been used for the detection of hydrocarbons as plastics (Driedger et al., 2013; Hasituya et al., 2016; Högig et al., 2010; Kühn et al., 2004; Novelli and Tarantino, 2015; Pichel et al., 2012; Slonecker et al., 2010), but not for AMD in the natural environment with high spatial resolution satellite imagery. It should be noted that to support the proper identification of each cover, supervised classifications require training data with valuable spectral information (Egorov et al., 2015).

Considering plastics as the usual AMD type, and its different size classes: microplastics (1 to < 5 mm), mesoplastics (5 to < 25 mm), and macroplastics (> 25 mm) (Barnes, 2002; Lee et al., 2013), the main objective of this work is to estimate the amount of macroplastics AMD on beaches through the use of very high spatial resolution imagery, and the hyperspectral characterization of AMD in the laboratory. Here we present an application to determine the amounts of AMD in a large scale over the Island of Chiloé, generating coastal maps of AMD, information that may be used for debris management strategy in the coordination of beach cleaning and decision making regarding the current status of AMD in Chiloé.

2. Study area and data

The Chiloé Archipelago is located in the northwestern area of Chilean Patagonia as an extension of the coastal mountain range located between 41° 48'–43° 22' S and 74° 14'–73° 20' W, approximately. The Isla Grande de Chiloé is separated from the mainland by the Gulf of Ancud to the east, by the Corcovado Gulf to the south, and is surrounded by the Pacific Ocean to the west. Tourism and fishing, especially aquaculture, have become prevalent on the island of Chiloé as a result of the local economic growth, which has led to a major shift in human settlements and to the expansion of the population limits, with insufficient land planning that might provide adequate accessibility and connectivity (Andrade et al., 2000).

The climate in the area is temperate and humid, with increased rainfall and maritime influence towards the southern and western parts of the island. The annual precipitation for Isla Grande is 2073 mm, spread out over the year with maximums in the winter months. The meteorological station in the provincial capital Castro records an accumulate average of 1891 mm per year (74–289 mm in February and June respectively) and an average temperature of 10.5 °C (14–6.8 °C in the months of January and July) (Pesce and Moreno, 2014).

For this work, we selected the inner sea of Chiloé which includes Detif, Punta Apabón, and Punta Mallil-Cuem beaches located in the communes of Puqueldón and Quinchao, respectively, both in the Los Lagos Region (Fig. 1). The sector has been recognized by the Aquatic Environment group of the Dirección General del Territorio Marítimo y de Marina Mercante (“General Directorate of Maritime Territory and Merchant Marine”) (DIRECTEMAR, 2014, 2016), as a site of coastal debris accumulation (DIRECTEMAR, 2014, 2016).

3. Method

3.1. Sample collection

Between January and February 2017, fieldwork was carried out on the beaches in the study area by collecting various AMD macroplastics, such as Styrofoam, plastic buoys, ropes, general plastics (e.g. bottles, containers, fragmented plastics) and any other type of object with a coverage > 0.5 m². These AMD selection criteria were estimated in campaigns through frequency, abundance and superficial area, from the intertidal zone until the presence of dense vegetation (ending of a stone-sand substrate). In addition, samples of natural elements such as algae, sands, stones and shells were acquired to characterize the natural substrate on the beaches. Over 144 samples were collected on the beaches of Punta Mallil-Cuem, Detif and Punta Apabón, as shown in

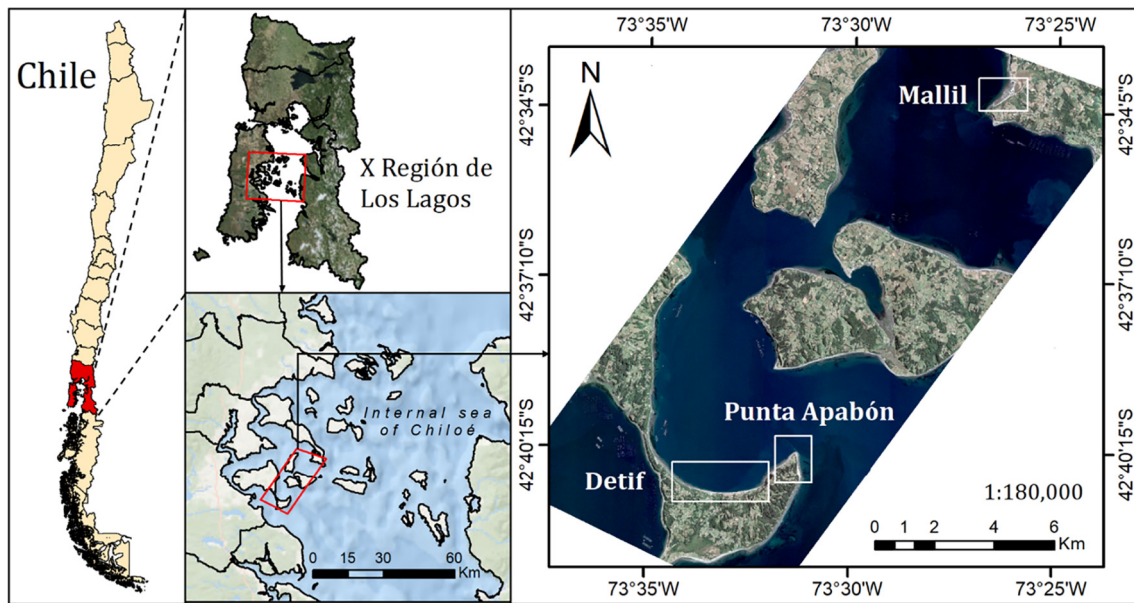


Fig. 1. Study area for the Chiloé islands highlighting the test sites of Detif, Punta Apabón and Punta Mallil-Cuem.

Table 1, they were characterized, labeled, some of them geo-referenced (accumulations), and carefully moved inside sealed boxes, to be analyzed later in the laboratory. The inert substrate samples were taken at the center of the squares defined by the stratified sampling method, at < 10 cm deep.

3.2. Laboratory measurements and spectral library

All the acquired samples were characterized by size, weight, density and color. Their spectral signatures were acquired in the laboratory using a HyLogger 3 reflectance spectrometer system (HL3™; Huntington et al., 2010), which has an integrated suite of hardware for the acquisition and analysis of spectral signatures (e.g. TSG software) in a linear and continuous 4 mm wide track and is unique in South America. The hardware has three sensors with spectral resolutions of 4 nm in the visible-near infrared (VNIR) [380–1000 nm] and short-wave infrared (SWIR) [1000–2500 nm], and 35 nm spectral resolution in the thermal infrared [6000–14,500 nm] (TIR), while also providing a height of the samples profile via a laser profilometer, and high resolution RGB images of the samples analyzed (Schodlok et al., 2016). This system was developed by CSIRO (2016) in Australia and is specifically designed to automatically detect mineralogy in drill core logging, though its versatility allows it to capture spectral signatures of any material, which can then be exported into data sheets for processing on other platforms (Schodlok et al., 2016).

The resulting spectra were compared to those obtained through the spectral instruments PS-300 from APOGEE® (PS300) for the VNIR range, and TerraSpec 4 Hi Res from ASD Inc. (TS4) for the VNIR-SWIR range. The integrated use of the mentioned instruments allowed the creation of a spectral database generated from the different instruments, in order to establish a comparison in terms of spectral and spatial resolution, enabling the validation of the spectral measurements acquired in the field through a quantitative assessment with those obtained in the laboratory.

Processing the acquired information involves performing a comparative data assessment, since there may be anomalous spectra due to different phenomena such as edges or unwanted pollutant material covering the instrument field of view. The multiple spectra (10 repetitions) of each sample were filtered according to mean and standard deviation criteria, enabling a better identification of the AMD spectral patterns. For the generation of the reference spectral library for the

different types of AMD, the same filter was applied between the signatures of the samples in the same category. In this analysis, the statistical criterion of standard deviation (SD or σ) was used for each wavelength and the anomalous acquisitions falling outside the range of the average ($\bar{X} \pm 1 \text{ SD}$) obtained through Eqs. (1) and (2), respectively, were discarded.

$$\bar{\rho}_{\lambda} = \frac{1}{n} \sum_{i=1}^n \rho_{\lambda i} \quad (1)$$

$$SD_{\rho} = \sigma_{\rho} = \sqrt{\frac{1}{n-1} \sum_{i=1}^n (\rho_{\lambda i} - \bar{\rho}_{\lambda})^2} \quad (2)$$

where, $\bar{\rho}_{\lambda}$: is the average of the sampling spectrums for a given wavelength (λ), $\rho_{\lambda i}$: is the reflectance measured for the spectrum i of the AMD sample category, n : is the number of spectra acquired for the sample, SD_{ρ} : is the standard deviation of the n spectra of the AMD sample.

Additionally, a comparison was performed between PS300, TS4 and HL3™ by calculating the Difference of the Amplitude “D” (Eq. (3)) as proposed by Price (1994), which was used to measure the difference percentage between the two spectra obtained by different sensors within a given spectral region.

$$D = \left[\frac{1}{\lambda_b - \lambda_a} \int_{\lambda_a}^{\lambda_b} [S1(\lambda) - S2(\lambda)]^2 d\lambda \right]^{1/2} \quad (3)$$





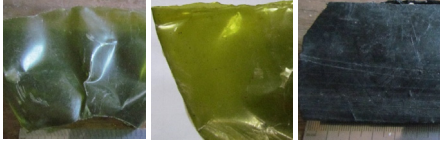

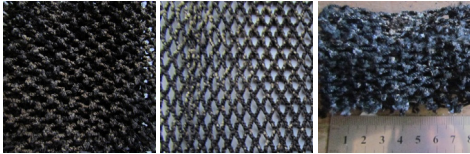




where, S1: is spectrum A for a given wavelength λ , S2: is spectrum B for a given wavelength λ , λ_{b-a} : Spectral wavelength or band [nm].

3.3. Image processing

A WorldView 3 (WV3) scene acquired on February 25, 2017, was used in this work. This image covers an area of 163 km², 8 bands in the VNIR spectral region (Coastal, Blue, Green, Yellow, Red, Red Edge, Near-IR1 and Near-IR2) and the panchromatic band (PAN), which has a spatial and radiometric resolution of 1.2 m for 14 bits, and 0.3 m for 11 bits, respectively.

The image was corrected atmospherically using the Atmospheric Compensation algorithm from DigitalGlobe (AComp; Pacifici, 2016). This recent algorithm has been used in high resolution imagery (Matasci et al., 2015; Pacifici et al., 2014) and compared to the well

Table 1
Manmade AMD and natural samples collected from the study area.

Type	No. samples	Image
Buoy	18	
Nautical rope	15	
Rope	13	
Mesh	4	
Plastic	8	
Styrofoam	25	
Total	83	
Netting	4	
Bag	17	
Shell	4	
Sand	30	
Rocks	6	
Total	61	

know methods FLAASH (Matthew et al., 2000) and QUAC (Bernstein et al., 2012), showing that in general AComp have more accuracy over different surfaces like asphalt, concrete, dirt, grass, sand, deep water and superficial vegetation in water (Pacifi, 2013) and a better performance for the identification of tree species (Cross et al., 2018). Subsequently, the surface spectral reflectance was estimated according to Eq. (4) and based on the data processing suggested by DigitalGlobe (Inc).

$$\rho_k = \frac{ND_k}{\max(ND_k)} \quad (4)$$

where, ρ_k : Reflectivity in band k . ND_k : Digital level in the band k .

3.4. Spectral signature convolution for satellite modelling

The hyperspectral spectra were convolved using RSRCalculator® to estimate the AMD reflectance values for the spectral bands corresponding to different remote sensors (Durán-Alarcón et al., 2014). This allowed to compare the spectral signatures measured in laboratory for each AMD, with the surface reflectance from WV3. The RSRCalculator® uses a weighted spectral convolution for each spectral band (C_k) (Eq. (5)) to calculate the value acquired from the spectral signature.

$$C_k = \frac{\int_{-\infty}^{+\infty} (rsr\lambda)(\rho\lambda)d\lambda}{\int_{-\infty}^{+\infty} (rsr\lambda)d\lambda} \quad (5)$$

where, C_k : Value obtained for the spectral convolution for band k , rsr_λ : is the relative spectral response of the band, ρ_λ : is the spectral signature under analysis, λ : Wavelength.

3.5. Image classification

3.5.1. AMD zone delimitation

The amount of AMD was identified on the high tide line, avoiding the spectral influence of large surfaces such as vegetation and sea. This procedure was carried out using a digital supervised classification to identify the surfaces, vegetation, and the intertidal zone. Photointerpretation points were generated to represent the spectral footprint of each surface and to delimit the specific sector of the intertidal zone on each beach. Regarding the number of sampling points (pixels) for digital classification, Foody and Mathur (2004b) point out that for multispectral images, a range of 25 times the number of spectral (variable) bands involved in the classification is generally used. However, if clear spectral differences are recognized between the surfaces under analysis, a smaller number of sampling points can be selected because this would basically provide the same accuracy as a greater number of points (Huang et al., 2002). Therefore, for each class, 90 pixels were selected from the scene to develop a supervised classification model. For this purpose, suitable and recommendable methods are Support Vector Machines (SVMs), algorithms that has shown higher accuracy and best adapted to small sample sizes as compared to traditional classification techniques such as decision trees, neural networks or conventional probabilistic methods (Foody and Mathur, 2004b; Huang et al., 2002). To complement the digital classification, an analysis of the distances between the high tide line and vegetation was performed because of the proximity of certain coastal zones to populated areas, which contain surfaces that might confuse the predictive model (e.g. zinc roofs, rural roads, Styrofoam in use or storehouse).

3.5.2. AMD spectral features and classification

A spectral separability analysis of the different materials collected was performed under controlled laboratory conditions. This analysis represent a key step to assess the ability to map the different classes of AMD by remote sensing, where each class must be assumed to have a unique and different spectral signature (Cho et al., 2009; Cochrane, 2000; Price, 1994). The spectral separability and unique spectral

features of each AMD class were determined using the Spectral Amplitude Difference metric (Eq. (3)) (Féret and Asner, 2011).

For AMD digital classification over beaches under study, the convolved spectral signatures from the WV3 (Eq. (5)) were used to train non-parametric methods such as Support Vector Machine (SVM) and Random Forest (RF), which have certain comparative advantages since they do not assume any representative statistical distribution of training data (e.g., average, variance) and often have greater classification power with small data sets (Belgiu and Drăguț, 2016; Foody and Mathur, 2004a; Huang et al., 2002; Pal, 2005; Rodríguez-Galiano et al., 2012). SVM is a model that classifies the data set using a Kernel type vector function, establishing and adjusting the separability limits between the categories under analysis (Kuhn and Johnson, 2013). This algorithm is extremely flexible because it allows different Kernel (e.g. Linear, Radial) and tuning parameters. With regards to RF method (Breiman, 2001), it consist in an algorithm for machine-learning classification based on decision trees, which has been used in remote sensing with excellent results in the classification of vegetation species, land cover and other types of surfaces (Immitzer et al., 2012; Pal, 2005; Puissant et al., 2014). This would facilitate satellite classification of AMD on beaches because this algorithm does not rely on previous knowledge of the statistical distribution of the satellite data (Belgiu and Drăguț, 2016; Rodríguez-Galiano et al., 2012). We also use Linear Discriminant Analysis (LDA) which is an easily-implemented conventional parametric statistical technique (Bandos et al., 2009). LDA has been used in different studies for spectral discrimination of vegetation and surface cover in various ecosystems (Clark et al., 2005; Féret and Asner, 2011). Basically, this method builds a set of linear functions that best discriminate the defined classes by combining predictive variables in a way that the variance between classes is maximized compared to the variance within the same class (Fung et al., 2003).

3.5.3. Predictive model and validation

The development of a predictive classification model is an iterative process aimed at obtaining an accurate prediction using the data available (Kuhn and Johnson, 2013). For this reason, it is common for classification models to be tuned via re-sampling techniques; different data subsets are used to train the model and other, for their validation, with the objective of obtaining a true quantification of each method error results (Castro-Esau et al., 2006). To build the prediction model for AMD, a combined database of laboratory spectral signatures was used along with GPS control points obtained in the field campaigns (January, February, June and July of 2017). Then, the photo-interpreted points, WV3 imagery, and field survey were used to identify large agglomerations of AMD, such as expanded polystyrene, other debris and pixels of sand. Accordingly, the built database was separated into one subset for training (70%) and another for validation (30%), and the training data were re-sampled by cross-validation (10-fold) for different AMD categories. The performance of the digital classification methods was assessed using a confusion matrix, allowing a series of effective evaluation statistics.

3.6. Estimated AMD mass on study area

To estimate the mass of the AMD on beaches, a stratified sampling method was developed at different distances from the intertidal zone (Fig. 2). To do this, a grid scheme like the WV3 pixel was used to quantify the debris present in a certain area (1.2×1.2 m). On each sampling point, all AMD inside the grid was weight to determine a relative density of AMD. This method was repeated all along the beach and descriptive information was recorded, such as the spatial coordinate (GPS), the types of AMD identified, the weight, and photograph before and after the shifting, among others. This method enabled assessing the reliability of the AMD prediction algorithm and eventually estimating the total mass of AMD on the beach. The information was stored in a database created in Google Earth ("www.github.com/

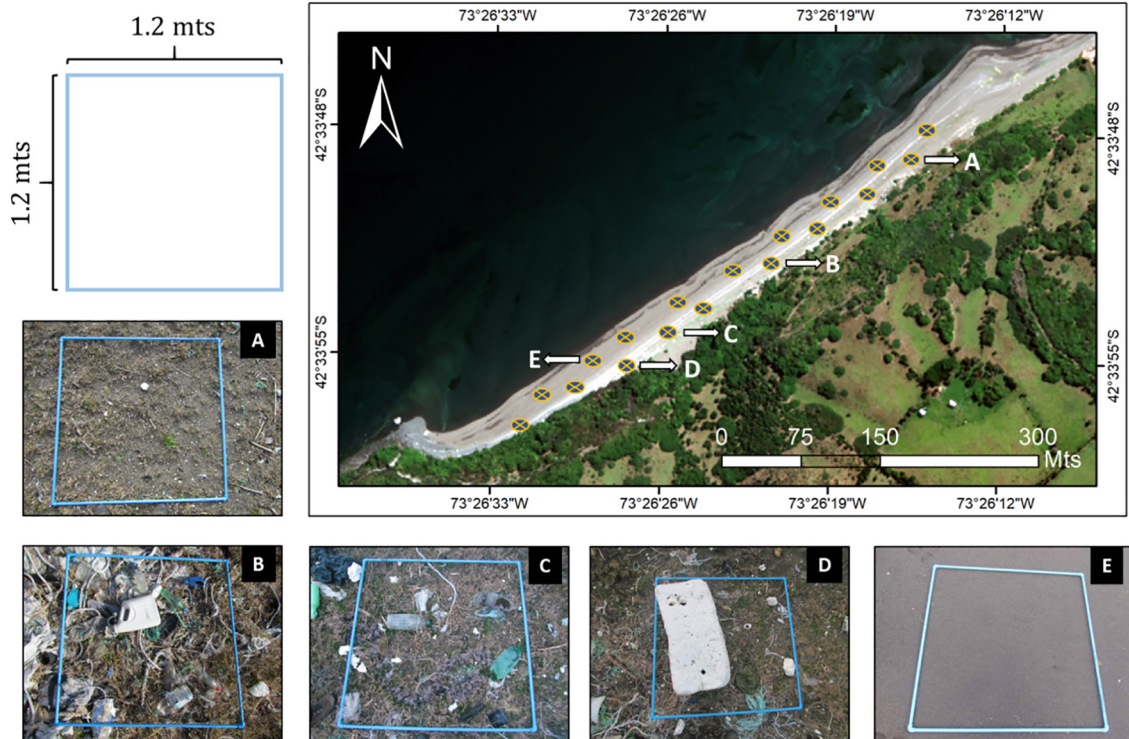


Fig. 2. Sample methods for AMD weight quantification over the Mallil-Cuem beach. Letters show different types and concentration of AMD such as, A) Without AMD, B) Ropes, Oil bottles, Ropes and meshes of aquaculture, among others, C) Pet bottles and other plastics, D) Styrofoam and plastics materials and E) Sand.

Labuchile/PREDRES”), which represents the sampling location points with photos of the AMD and metadata.

Finally, Fig. 3 summarizes the proposed methodology in four steps, including the (1) Data Acquisition, obtaining the satellite image and ground truth data which included the AMD samples, GPS points of AMD accumulation, and the grid sampling method for the posterior mass

determination. The (2) Data Processing and Algorithm Construction incorporates the generation of the AMD Spectral Library, the organization of all the ground truth data, the corrections of the satellite image and the application of the supervised classification methods. The next step (3) a Validation of the AMD classification were performed, including an iteration of the model for a broader understanding in the

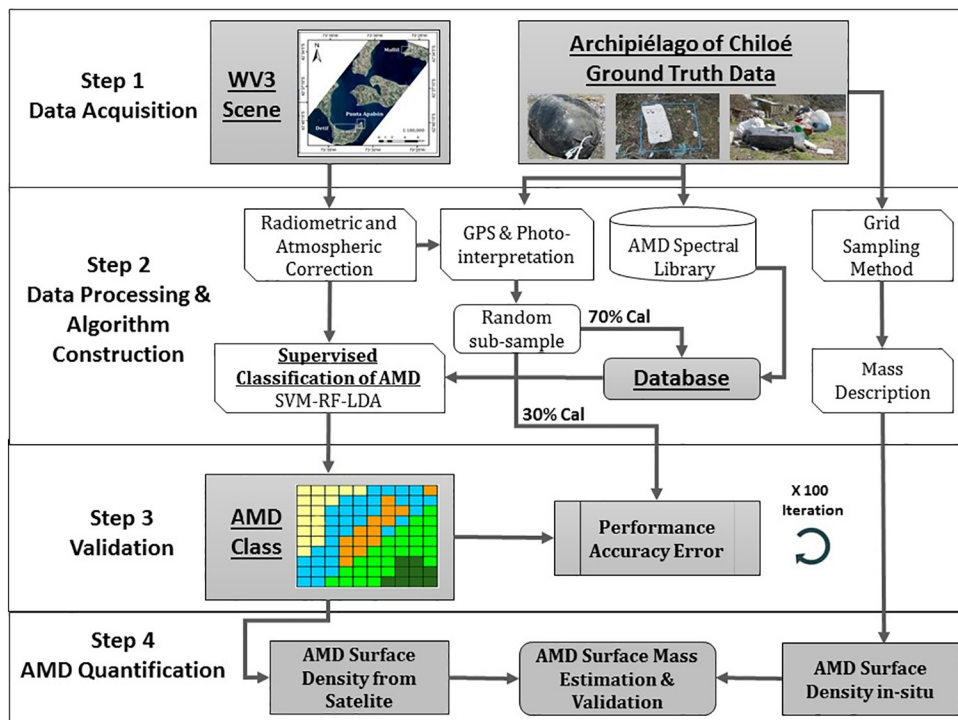


Fig. 3. Flowchart for AMD classification over Chiloé beaches.

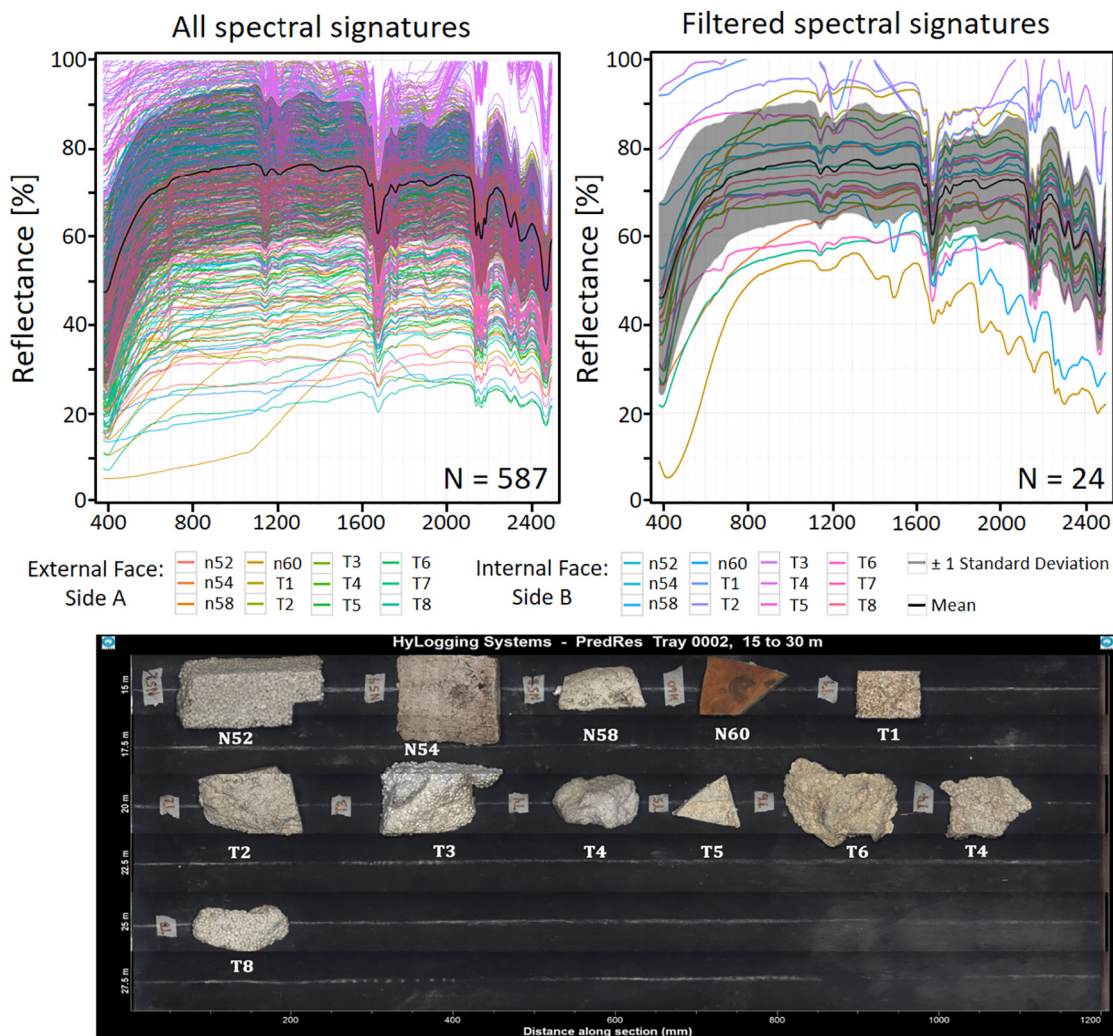


Fig. 4. Spectral signatures and images acquired by HyLogger 3. Top: Different samples of Styrofoam collected from field campaign. Left: non-filtered spectral signatures. Right: Filtered spectral signatures of each samples with mean ± 1 standard deviation. External Face (Side A): correspond to the side of the sample collected in the beach undergone environmental weathering. Internal Face (Side B): correspond to an inner cut of the same sample which has not suffered environmental exposure.

performance of the accuracy errors. Finally, (4) AMD Quantification, estimation using the mass description collected at in-situ, in order to quantify the AMD Surface Mass for the entire beaches.

4. Results

4.1. Spectral data base

The spectral signatures acquired by HL3™ were processed and sorted in a database for digital classification of the images. First, the multiple spectral signatures of each sample were filtered, and then the signatures of all the samples of the same AMD class were again filtered (Fig. 4, example for Styrofoam). There was a wide variability among samples analyzed throughout the range of VNIR (380–1000 nm) and SWIR (1000–2500 nm), which matches with their variability in dirt, color, water content, biofouling and other environmental weathering processes (e.g. solar irradiance, air humidity, winds). Some of the samples had high variability between their own surfaces, and in that case, we separated them in two different sides (treated as different samples), in order to include this variation in the AMD spectral library. The external face (Side A) corresponded to the surface affected by the variety of environmental weathering processes, also with scratches and different roughness, and the internal face (Side B), corresponded to an

inner cut of the samples, without direct environmental exposure and a relative flat surface (Fig. 5). The standard deviation filter had a significant effect on the elimination of spectral signatures with extreme values, which may be result of small roughed areas in the samples that overestimated reflectance. For Styrofoam, reflectance increased progressively by 30% between 380 and 680 nm and then an average value of 72% in the NIR (700–1000 nm) and 68% in the SWIR (Fig. 4). Additionally, in the SWIR range, there were spectral features of differentiated absorption appearing in the regions of 1670–1690 nm, 2130–2190 nm and 2430–2500 nm (Fig. 4).

It should be noted that the available WV3 satellite information only covers the VNIR spectral region, which means subsequent analyses only considered wavelengths between 400 and 1100 nm.

The degree of similarity between the internal and external face of each Styrofoam sample obtained with HL3™ was analyzed. To do so, the difference in spectral amplitude (D, Eq. (3)) was calculated for the VIS (D_{vis}) and NIR (D_{nir}) regions, which for the total 24 Styrofoam samples analyzed, gave an average value of 20% and 15%, respectively. This variability existed mainly between 380 and 680 nm, for example, sample N58 had a D_{vis} value of 19% (D_{nir}, 10%), for N60 there was a spectral difference of 31% for D_{vis} (D_{nir}, 13%), in the case of sample N54, a D_{vis} value of 23% was obtained (D_{nir} 17%) and finally for sample T5, a D_{vis} value of 25% (D_{nir} 5%) (Fig. 5). These differences

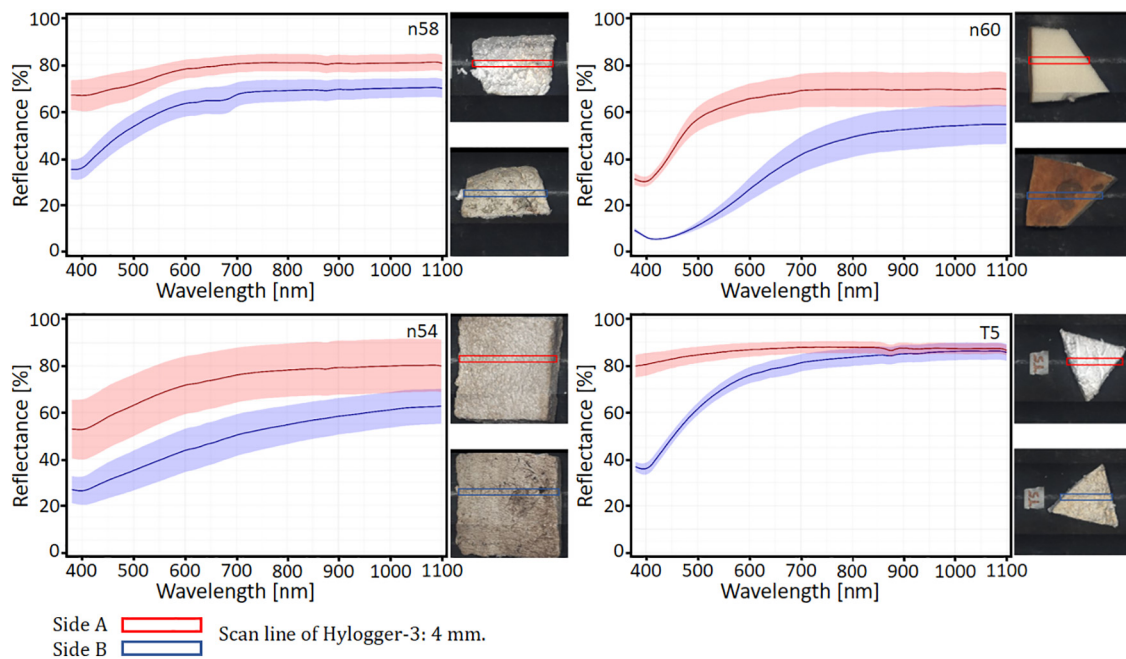


Fig. 5. Comparison of internal and external face of four different Styrofoam samples affected by environmental weathering such as N58: Dirt and physical damage; N60: Solar radiation; N54: Dirt, water and solar radiation; T5: Inlay dirt and microorganism.

were also found in all the analyzed Styrofoam samples, in which a potential feature in the NIR region for spectrally separating Styrofoam was identified.

4.1.1. Results of spectral signature processing

The processing and analysis of the spectral signatures generated by HL3™, as well as the data filter by standard deviation, was performed on all the materials collected in the study area (Fig. 6, left). The spectrally convolved value was then estimated for the different types of AMD, obtaining a boxplot graph associated with the reflectance variability in WV3 bands (Fig. 6, right).

Buoys corresponded to high density polyethylene material with a low reflectance in the VNIR (< 20%). This AMD is widely used in mussel farming and others, and can be found in different colors, resulting in its variation in the same part of the spectrum. In the NIR region, on the other hand, it showed a spectral absorbance pattern in the 930 nm band for all the evaluated samples. Ropes had a variable spectral pattern with a reflectance below 35% in the VNIR and a minimum SD of 5% in NIR. At the same time, the boxplot (right) clearly corresponded to the sectors with the highest spectral variability in the signature according to the interquartile deviation (yellow, red and red edge bands). The Nets (aquaculture nets) had a reflectance under 10% between 400 and 500 nm, which increased to 15–20% in the remaining bands. The particular case of Other Plastics, corresponded to fragmented black plastic pieces together with PET bottles and other transparent materials, resulting in a low reflectance (5–7%) with a minimal variability (< 3%) for the entire analyzed spectrum. Styrofoam presented the highest reflectance (40–70%) of all the types of AMD, with a persistent variation of ~10% related directly to the multiple processes of environmental degradation that may affect its reflectance. Sacks had the most variable reference spectral signature, with up to a ~10–15% amplitude between the 510 and 780 nm range caused by the various coloration and levels of wear, as also occurs in the Buoys. In the case of the Sand, its spectral signature was characterized by low and constant reflectance (< 10%), attributable to the moisture content of the samples acquired in the coastal area.

The AMD spectra signatures were convolved according to the WV3 band spectral response function (Fig. 6, right). In comparison, Styrofoam had clear spectral difference to the rest of the AMD materials

analyzed, and thanks to its high reflectance, it is differentiable at the WV3 imagery level. Instead, the remaining AMD materials studied showed low spectral amplitude and high dispersion in the spectral region analyzed. This is attributed to the level of degradation and chemical characteristics causing a significant overlap in the VNIR bands, thus making it impossible to spectrally separate it at WV3 scale (Fig. 7A).

4.2. Digital classification

Results of the spectral processing showed that it was not possible to spectrally classify all the AMD separately due to their great variability in the WV3 bands (Fig. 7A), and even more, by their lack of pixel representation in the WV3 scene for each type of AMD. However, Styrofoam had a unique spectral characteristic compared to other AMD materials and enough representation in the study area, thus the digital classification could be performed separately for this type of AMD. Therefore, the categories classified corresponded to Expanded Polystyrene AMD (Styrofoam), and AMD Mixture, which corresponds to the other types of AMD together (Fig. 7B).

The supervised classification was done with the methods Random Forest, Linear Discriminant Analysis and Support Vector Machine, the last with 3 different kernels (Linear, Radial and Polynomial) (Fig. 8).

For Punta Apabón beach, the best method corresponded to SVM Linear, with an overall accuracy of 91% and Kappa index of 84%. In this sector, there were big accumulations of Styrofoam among the debris dispersed on a beach made of stones (1.5–3 cm in diameter). Punta Mallil-Cuem beach had overall results above 80% in all the methods, with maximums for LDA, RF and Radial SVM (88%). This is attributed to a fine white sand and greater presence of herbaceous vegetation in the high tide section. As for Detif beach, an overall accuracy of 83% was achieved with SVM Linear, detecting high concentration of AMD along the high tide line on a 3 m wide strip, mainly of Styrofoam debris, fishing ropes and household litter. Lastly, the Matao validation beach performed well in the classification, with values over 80% in the best cases (RF and Linear and Radial SVM), but with poor Kappa index results, which might be directly related to lower availability of testing data. Nevertheless, low concentrations of AMD in the field were confirmed.

In general terms, the accuracies of the different AMD classification models were > 75%, depending basically on the data selected for calibration and validation. To evaluate which of the five predictive methods perform consistently better, 100 iterations of the classification on the Mallil-Cuem beach were made, with the data being randomly sub-sampled in each case (Fig. 9). Radial SVM corresponded to the classification method with the best overall accuracy on average, having it higher frequency close to 90%.

4.3. Mass determination

The estimation of AMD concentration on each beach was performed by taking the WV3 pixel area and the average density of styrofoam (38.16 kg/pixel) and of an AMD mixture (1.75 kg/pixel). A summary of

the mass determination for each beach (Table 2), showed that Detif was the one with the highest AMD mass, with an average of 26.85 tons and a standard deviation of 8.8 tons, directly related to the extension of the beach (~4 km), however, it also has the greatest amount of AMD per area, with a maximum of 0.692 kg/m² estimated with SVM Polynomial. Punta Apabón and Mallil-Cuem beaches had an average concentration of 8.29 and 6.67 tons and a standard deviation of 2 and 1.6 tons, respectively, with a maximum of 0.447 and 0.248 kg/m². Lastly, Matao beach had the lowest average concentration of AMD, with 1.89 tons and a standard deviation of 0.8 tons, estimating 0.137 kg/m² with Random Forest.

The variability observed in the prediction of the models is primarily linked to the estimates made with LDA, given that they have a marked difference with the remaining classification methods, with the

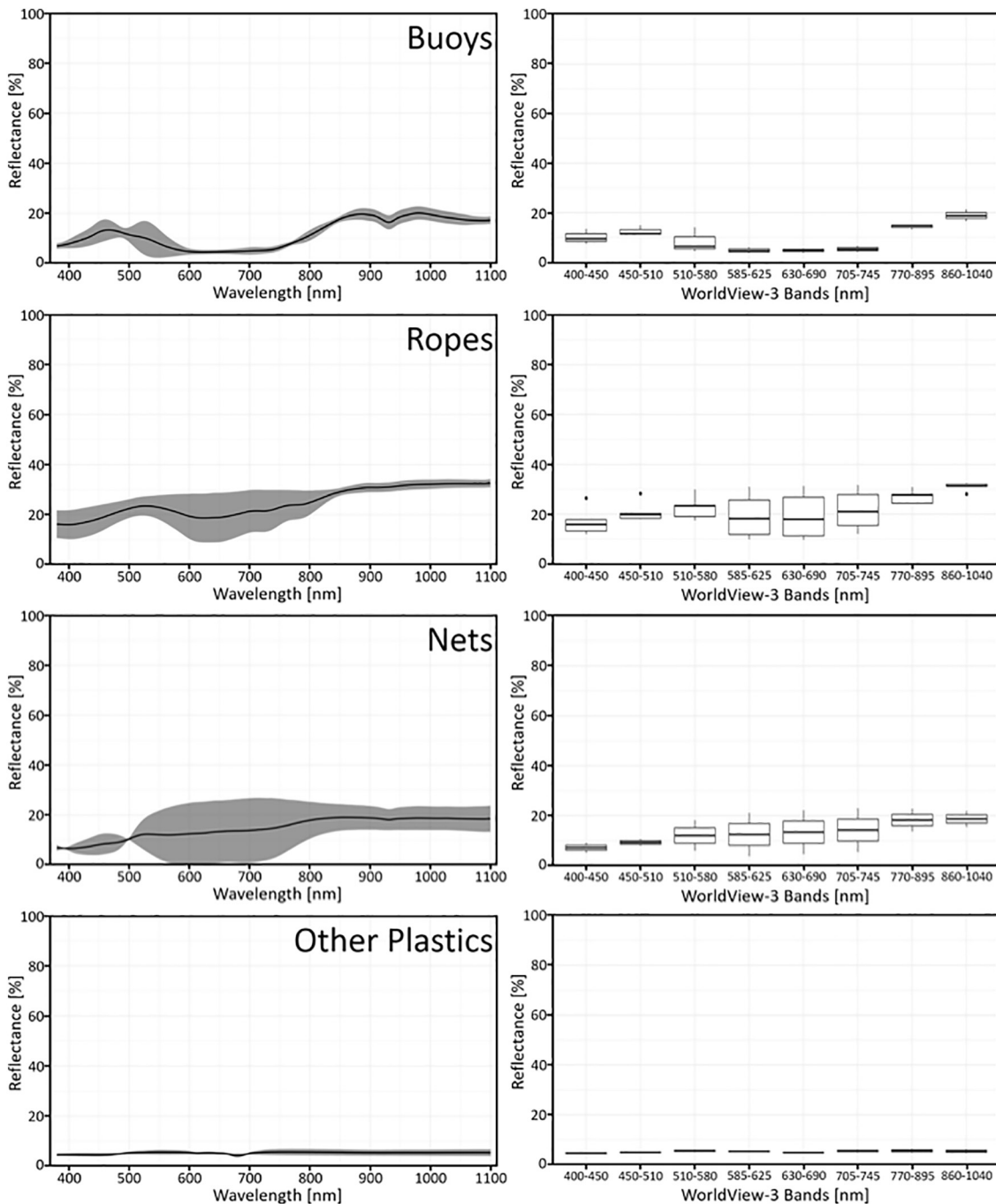


Fig. 6. Representative spectral signatures (left) and WV3 convolution boxplot (right) of different types of AMD and sand.

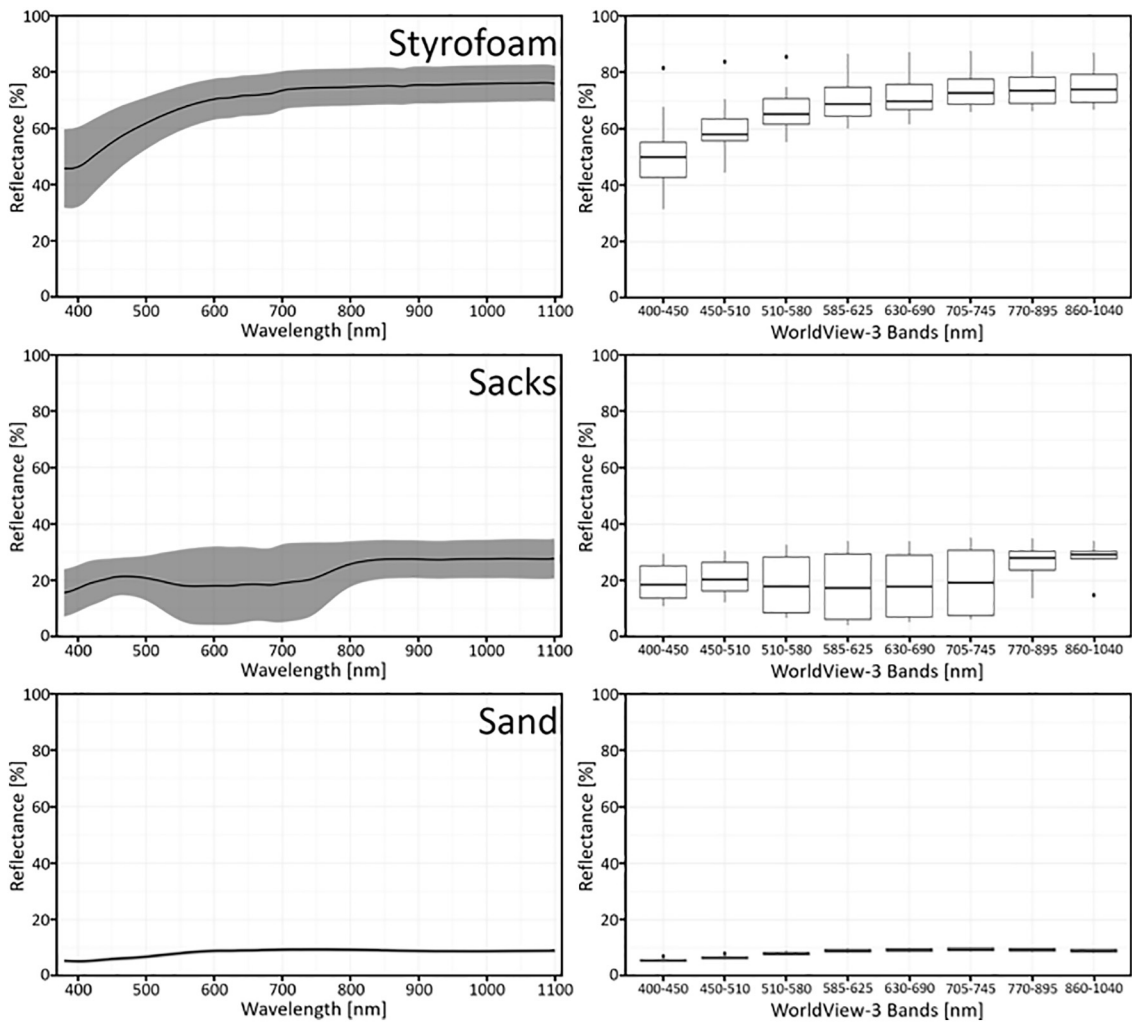


Fig. 6. (continued)

exception of Mallil-Cuem beach. This might be related to the structure of the method, which has a standardized linear statistical mechanism and depends on the amount of input data, which produces a method that over-fits to the training and validation data.

5. Discussion

The acquisition of spectral signatures of AMD is crucial for improving their identification on beaches using satellite images. The

spectral characterization in laboratory allows the application of digital classification algorithms on images acquired by multispectral sensors onboard satellites, aircraft and others UAV. This create the opportunity to automatize the identification of AMD, reducing efforts and time, and becoming one of the first studies to successfully quantify macroplastic marine debris in a multispectral and high resolution image.

The current satellite missions provide the opportunity to choose from a wide range of sensors designed to meet objectives according to the spatial and spectral characteristics, and the revisit time on the area

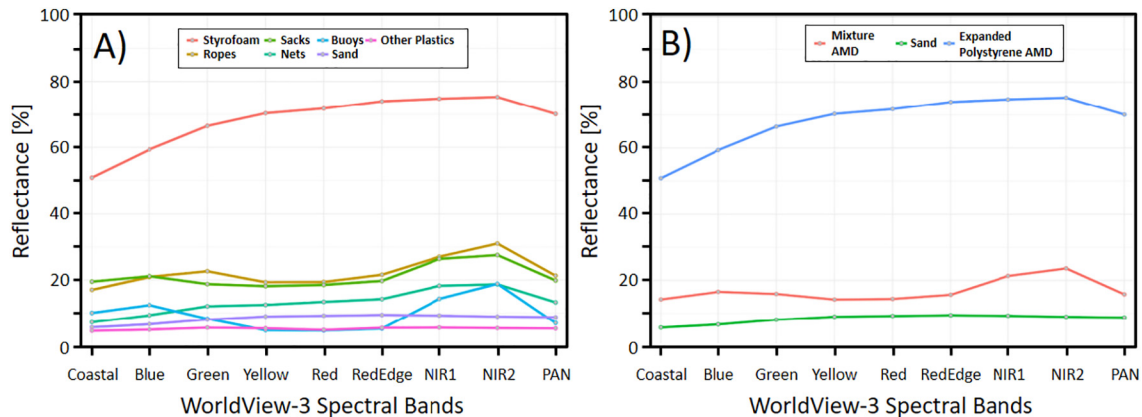


Fig. 7. (A) Normalized spectral signatures of the different types of AMD in terms of WV3 Bands. (B) Final spectral classes used as input in the classification.

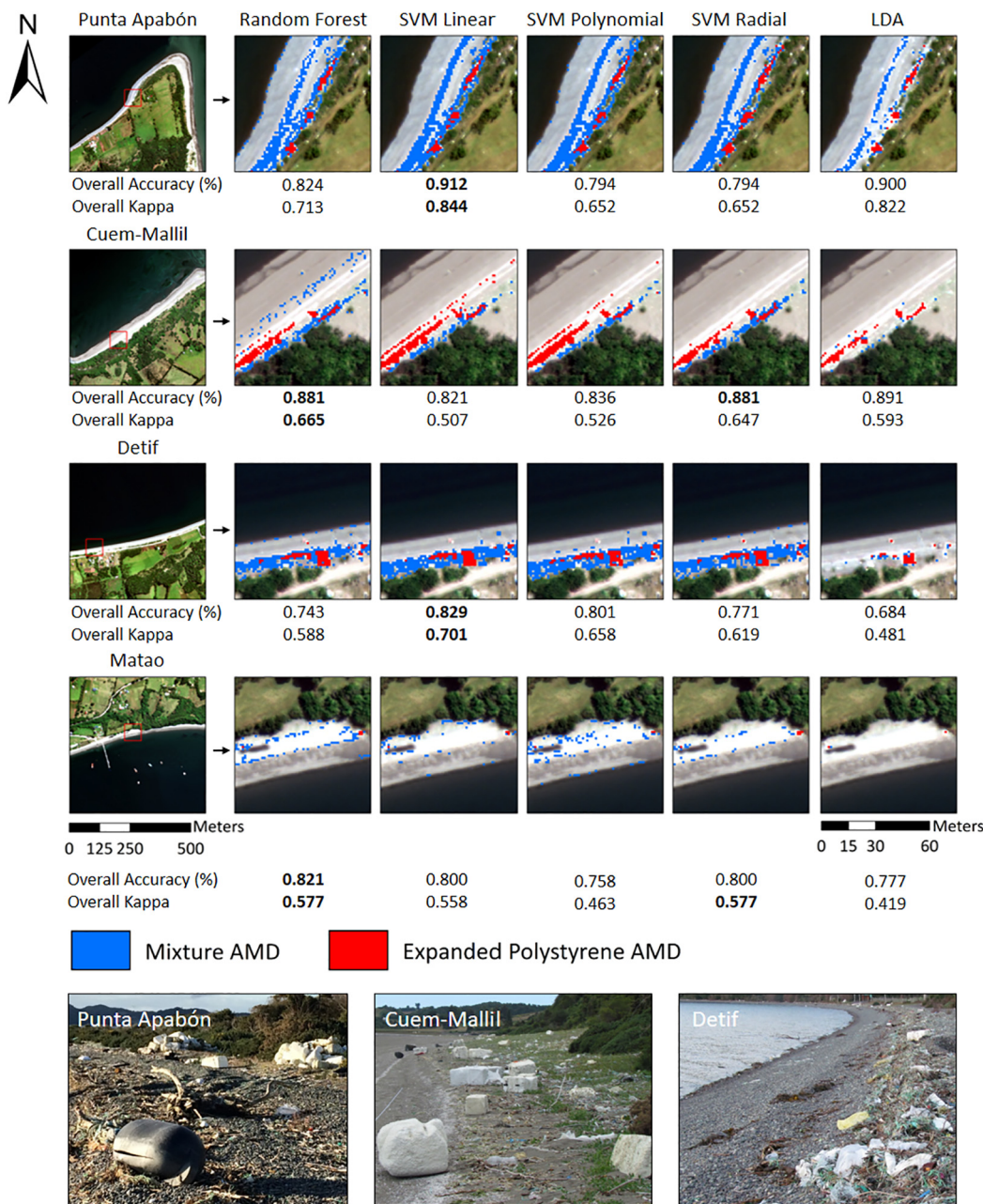


Fig. 8. Supervised classification assessment over Punta Apabón, Mallil-Cuem, Detif and Matao beaches. Highest overall accuracy and kappa indexes are also shown.

of interest. The high level of spatial and spectral details obtained from WV3 imagery is essential for identifying and classifying AMD in the territory of Chiloé. However, the climate in the study area is heavily influenced by its coastal location and high moisture content, resulting in low availability of cloud-free scenes and the need for robust atmospheric corrections in order to minimize the effect of marine and terrestrial aerosols on the results.

Due to the diversity of substrates where AMD are usually deposited, some factors that might affect classification are the type of sand-soil or clast on the beaches under analysis, where anything from round rocks to fine sand can be found. This could affect the spectral contrast existing between the reflectance of the sand, the AMD mixture and the Styrofoam, affecting the ability to classify properly. Therefore, it becomes necessary to take in account a spectral signature of the substrate where the AMD classification is to be carried out.

Regarding the performance of the predictive models, it was demonstrated that AMD digital classification is feasible, and its accuracy

mainly depends on the calibration and validation data of the supervised methods. For this study, however, a combination of different analytical methods of digital supervised classification was carried out, thus reducing any uncertainty associated with the methods thanks to a series of iterations. This technique of iteration and reduction in classification error has been used to create bioclimatic models of plant species distribution (Thuiller et al., 2009, Engler et al., 2011, Araújo and New, 2007) and mapping of tree species (Engler et al., 2013).

A similar AMD study is presented by Garaba and Dierssen (2018), identifying specific absorption features in the spectral signatures of microplastics, although their samples did not reveal being affected by environmental exposure, such as surfactants and biofouling. The samples collected in this work were affected in a wide range of organic matter, biofouling and environmental weathering. Therefore, the AMD spectral signature generated in this work mostly represent the actual debris to be founded in the beaches of Chiloé, making possible the aggregation of several spectra in a “bulk” signature that was applied for

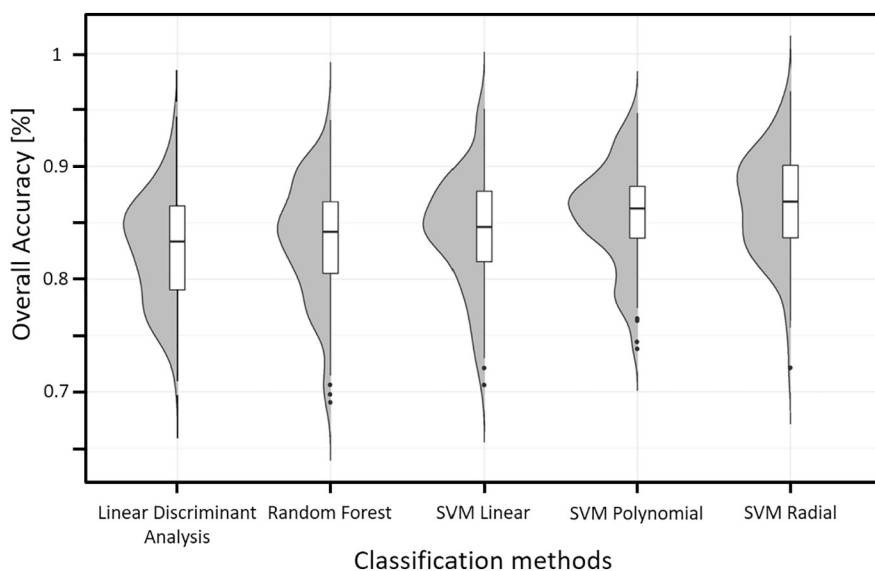


Fig. 9. Distribution plot of 100 iterations assessment for each classification method over Mallil-Cuem beach.

Table 2
Summary for each beach and its estimation of mass for the five classification methods.

Test site	Classification method	Area [m ²]			[Tons]			[kg/m ²]
		Beach extension [m]	Expanded polystyrene	Mixture AMD	Expanded polystyrene	Mixture AMD	Total	
Punta Apabón	Random forest	21,232.80	207.36	3186.72	5.495	3.885	9.380	0.442
	SVM linear		204.48	3000.96	5.419	3.658	9.077	0.427
	SVM polynomial		201.60	2851.20	5.342	3.476	8.818	0.415
	SVM radial		269.28	1936.80	7.136	2.361	9.497	0.447
	LDA		142.56	743.04	3.780	0.910	4.680	0.220
Mallil-Cuem	Random forest	35,972.60	216.00	1389.60	5.724	1.694	7.418	0.206
	SVM linear		162.72	1307.52	4.312	1.594	5.906	0.164
	SVM polynomial		149.76	570.24	3.969	0.695	4.664	0.130
	SVM radial		298.08	840.96	7.899	1.025	8.924	0.248
	LDA		231.84	276.48	6.140	0.340	6.480	0.180
Detif	Random forest	44,926.60	479.52	10,038.24	12.707	12.238	24.945	0.555
	SVM linear		545.76	11,344.32	14.463	13.830	28.292	0.630
	SVM polynomial		714.24	14,656.32	17.477	13.616	31.093	0.692
	SVM radial		659.52	11,168.64	18.927	17.867	36.795	0.819
	LDA		360.00	2934.72	9.540	3.580	13.12	0.292
Matao	Random forest	19,175.00	27.36	1560.96	0.725	1.903	2.628	0.137
	SVM linear		21.60	1556.64	0.572	1.898	2.470	0.129
	SVM polynomial		21.60	1084.32	0.572	1.322	1.894	0.099
	SVM radial		53.28	515.52	1.412	0.628	2.040	0.106
	LDA		15.84	23.04	0.420	0.030	0.450	0.023

the classification in the imagery. This work contributes to better understand the high range of spectral signatures of AMD affected by weathering conditions which differs from the spectra directly obtained from virgin plastics.

Other research must be conducted to improve the knowledge of macroplastics spectra at varying the time of environmental conditions, the content of water, biofouling and dirt. In this context, the resolutions for SWIR in most satellites might allow an asset, although the SWIR of WV3 has a coarser resolution than the VNIR and NIR bands, making difficult its inclusion in the analysis and in the predictive model proposed in this work. Nevertheless, our results represent, as a first approach, a feasible predictive model which used a limited spectral and a high spatial resolution imagery, retrieving the location and extent of plastics in the natural environment, improving the actual state of remote sensing applications (Driedger et al., 2013; Hasituya et al., 2016; Hörig et al., 2010; Kühn et al., 2004; Novelli and Tarantino, 2015; Pichel et al., 2012; Slonecker et al., 2010). The proposed method can be automated and used for monitoring debris in beaches, periodically and with high accuracy, although some hyperspectral features of natural

surfaces are site dependent.

One of the most important results of this study is related to the decision making regarding to the AMD environmental problems on the Island of Chiloé. The results obtained are crucial for determining the minimum requirements for AMD transport and processing logistics as they can provide a priori knowledge of the loads to be collected, the area where the AMD are to be stockpiled and pre-treated. The economic and/or environmental transfer of this debris for reevaluation in the market or for its final disposal in landfills is another aspect where this work can add value, by providing the approximate mass of AMD accumulation on the beaches. However, some basic assumptions were made in estimating AMD density, such as the area covered by AMD in the WV3 pixel, and its relation to Styrofoam with an average height, which could be modified and adapted to other type of AMD.

6. Conclusions

This work presents a spectral characterization of anthropogenic marine debris identified on the beaches of Chiloé, Chile, which is then

applied in a digital supervised classification using very high-resolution satellite images. The spectral signatures obtained with the Hylogger-3 equipment allowed the spectral patterns of each AMD to be determined. Expanded polystyrene and AMD mixtures deposited on the beaches in images of 0.3 to 1.2 m spatial resolution could be detected with low error. One opportunity for improvement would be to include other ranges of wavelengths (spectral bands) that may enable the classification in adverse weather conditions, as well as distinguishing types of waste in AMD mixtures other than expanded polystyrene. The digital supervised classification methods employed in this work varied in their performance according to the type of substrate, remarkably with precision of 80% in general. This work provides new sources of information that might be applied to environmental problems associated to AMD on a global scale, making easier to create an environmental management strategy for coordinating beach cleaning and decision making regarding AMD monitoring in Chiloé.

Acknowledgements

This project was mainly financed with contributions from the Agencia de Sustentabilidad para el Cambio Climático (ASCC) by way of the project entitled: “Estudio para la generación de un modelo predictivo de residuos en 3 playas de Chiloé, mediante Teledetección Cuantitativa (PRED-RES Chiloé)” and the INNOVA CSIRO—CHILE 10CEII—9007 project (run by the HL3).

References

- Andrade, B., Arenas, F., Quense, J., 2000. Caracterización ambiental aplicada y ordenamiento del territorio: la costa oriental de la Isla Grande de Chiloé. In: *Revista de Geografía Norte Grande*. 27. pp. 123–132.
- Araújo, M.B., New, M., 2007. Ensemble forecasting of species distributions. *Trends Ecol. Evol.* 22, 42–47.
- Astudillo, J., Bravo, M., Dumont, C., Thiel, M., 2009. Detached aquaculture buoys in the SE Pacific: potential dispersal vehicles for associated organisms. *Aquat. Biol.* 5, 219–231.
- Bandos, T.V.V., Bruzzone, L., Camps-Valls, G., 2009. Classification of hyperspectral images with regularized linear discriminant analysis. *IEEE Trans. Geosci. Remote Sens.* 47, 862–873.
- Barnes, D.K., 2002. Invasions by marine life on plastic debris. *Nature* 416, 808–809.
- Barnes, D.K., Milner, P., 2005. Drifting plastic and its consequences for sessile organism dispersal in the Atlantic Ocean. *Mar. Biol.* 146, 815–825.
- Belgiu, M., Drăguț, L., 2016. Random forest in remote sensing: a review of applications and future directions. *ISPRS J. Photogramm. Remote Sens.* 114, 24–31.
- Bergmann, M., Gutow, L., Klages, M. (Eds.), 2015. *Marine Anthropogenic Litter*. Springer, Open.
- Bernstein, L., Jin, X., Gregor, B., Adler-Golden, S., 2012. The quick atmospheric correction (QUAC) code: algorithm description and recent upgrades. *Opt. Eng.* 51 (11), 111719.
- Bourne, W.R.P., Clarke, G.C., 1984. The occurrence of birds and garbage at the Humboldt front off Valparaíso, Chile. *Mar. Pollut. Bull.* 15 (9), 343–344.
- Brainard, R., Foley, D., Donohue, M., 2000. Origins, types, distribution, and magnitude of derelict fishing gear. In: *Proceedings of the International Marine Debris Conference on Derelict Fishing Gear and the Ocean Environment*. National Marine Sanctuaries, Hawaii, pp. 24–38.
- Bravo, M., Gallardo, M., Luna-Jorquera, G., Núñez, P., Vásquez, N., Thiel, M., 2009. Anthropogenic debris on beaches in the SE Pacific (Chile): results from a national survey supported by volunteers. *Mar. Pollut. Bull.* 58, 1718–1726.
- Breiman, L., 2001. Random forests. *Mach. Learn.* 45, 5–32.
- Castro-Esau, K.L., Sanchez-Azofeifa, G.A., Rivard, B., Wright, S.J., Quesada, M., 2006. Variability in Leaf Optical Properties of Mesoamerican Trees and the Potential for Species Classification. 93. pp. 517–530.
- Cheshire, A.C., Adler, E., Barbière, J., Cohen, Y., Evans, S., Jarayabhand, S., Jetic, L., Jung, R.T., Kinsey, S., Kusui, E.T., Lavine, L., Manyara, P., Oosterbaan, L., Pereira, M.A., Sheavly, S., Tkalin, A., Varadarajan, S., Wenneker, B., Westphalen, G., 2009. UNEP/IOC guidelines on survey and monitoring of marine litter. In: *UNEP Regional Seas Reports and Studies No. 186*. IOC Technical Series No. 83 (120 p).
- Cho, M.A., Debba, P., Mathieu, R., van Aardt, J., Asner, G.P., Naidoo, L., Main, R., Ramoelo, A., Majeke, B., 2009. Spectral variability within species and its effects on savanna tree species discrimination. In: *International Geoscience and Remote Sensing Symposium (IGARSS)*. Vol. II. pp. 190–193. <https://doi.org/10.1109/IGARSS.2009.5418038>.
- Chubarenko, I., Stepanova, N., 2017. Microplastics in sea coastal zone: lesson learned from the Baltic amber. *Environ. Pollut.* 30, 1–12.
- Clark, M.L., Roberts, D., Clark, D.B., 2005. Hyperspectral discrimination of tropical rain forest tree species at leaf to crown scales. *Remote Sens. Environ.* 96, 375–398.
- Cochrane, M.A., 2000. Using vegetation reflectance variability for species level classification of hyperspectral data. *Remote Sens. Environ.* 21 (10), 2075–2087.
- Convey, P., Barnes, D., Morton, A., 2002. Debris accumulation on oceanic island shores of the Scotia Arc, Antarctica. *Polar Biol.* 25, 612–617.
- Cross, M.D., Scambos, T.A., Pacifici, F., Marshall, W.E., 2018. Validating the use of metre-scale multi-spectral satellite image data for identifying tropical forest tree species. *Int. J. Remote Sens.* 39, 3723–3752.
- CSIRO (Commonwealth Scientific and Industrial Research Organisation) Australian Government, 2016. <http://www.csiro.au/>, Accessed date: 1 April 2016.
- Derraik, J., 2002. The pollution of the marine environment by plastic debris: a review. *Mar. Pollut. Bull.* 44 (9), 842–852.
- DIRECTEMAR (Dirección general del Territorio Marítimo y Marina Mercante), 2014. Desechos marinos en playas de jurisdicción de la gobernación marítima de castro. In: *Informe técnico No 2*. Dirección marítima de Castro, Chiloé.
- DIRECTEMAR (Dirección general del Territorio Marítimo y Marina Mercante), 2016. Desechos marinos en playas de jurisdicción de la gobernación marítima de castro: condición Octubre 2016. In: *Informe técnico No 3*. Dirección marítima de Castro, Chiloé.
- Driedger, A., Dürr, H., Mitchell, K., Flannery, J., Brancazi, E., Van Capellen, P., 2013. Plastic debris: remote sensing and characterization. (Sheboygan, Wisconsin, USA). In: *Lake Michigan: State of Lake Michigan and the 13th annual Great Lakes Beach Association Conference (2013)*, pp. 15–17.
- Driedger, A., Dürr, H., Mitchell, K., Van Capellen, P., 2015. Plastic debris in the Laurentian Great Lakes: a review. *J. Great Lakes Res.* 41, 9–19.
- Durán-Alarcón, C., Santamaría-Artigas, A., Valenzuela, N., Mattar, C., 2014. RSR Calculator, una herramienta para el proceso de calibración/validación. In: *Revista Española de Teledetección*. 42. pp. 111–117.
- Egorov, A., Hansen, M., Roy, D., Komareddy, A., Potapov, P., 2015. Image interpretation-guided supervised classification using nested segmentation. *Remote Sens. Environ.* 165, 135–147.
- Engler, R., Randin, C.R., Thuiller, W., Dullinger, S., Zimmermann, N.E., Araújo, M.B., Pearman, P.B., Albert, C.H., Choler, P., de Lamo, X., Dirnböck, T., Gómez-García, D., Grytnes, J.-A., Heegard, E., Hoistad, F., Le Lay, G., Nogues-Bravo, D., Normand, S., Pédalu, C., Puscas, M., Sebastià, M.-T., Stanisci, A., Theurillat, J.-P., Trivedi, M., Vittoz, P., Guisan, A., 2011. 21st century climate change threatens mountain flora unequally across Europe. *Glob. Chang. Biol.* 17 (7), 2330–2341.
- Engler, R., Waser, L.T., Zimmermann, N.E., Schaub, M., Berdos, S., Ginzler, C., Psomas, A., 2013. Combining ensemble modeling and remote sensing for mapping individual tree species at high spatial resolution. *For. Ecol. Manag.* 310, 64–73.
- Féret, J.B., Asner, G.P., 2011. Spectroscopic classification of tropical forest species using radiative transfer modeling. *Remote Sens. Environ.* 115 (9), 2415–2422. <https://doi.org/10.1016/j.rse.2011.05.004>.
- Foody, G.M., Mathur, A., 2004a. A relative evaluation of multiclass image classification by support vector machines. *IEEE Trans. Geosci. Remote Sens.* 42 (6), 1335–1343. <https://doi.org/10.1109/TGRS.2004.827257>.
- Foody, G.M., Mathur, A., 2004b. Toward intelligent training of supervised image classifications: directing training data acquisition for SVM classification. *Remote Sens. Environ.* 93 (1–2), 107–117. <https://doi.org/10.1016/j.rse.2004.06.017>.
- Fujieda, S., Sasaki, K., 2005. Stranded debris of foamed plastics on the coast of Eta Island and Kurahashi Island in Hiroshima Bay. *Nippon Suisan Gakkaishi* 71, 755–761.
- Fung, T., Yan Ma, H.F., Siu, W.L., 2003. Band selection using hyperspectral data of subtropical tree species. *Geocarto Int.* 18 (4), 3–11.
- Galgani, F., Fleet, D., Van Franeker, J., Katsanevakis, S., Maes, T., Mouat, J., Oosterbaan, L., Poitou, I., Hanke, G., Thompson, R., Amato, E., Birkun, A., Janseen, C., 2010. Marine strategy framework directive - task group 10 report marine litter. In: *Zampoukas, N. (Ed.), JRC Scientific and Technical Reports*. European Commission Joint Research Centre, Ispra.
- Gall, S., Thompson, R., 2015. The impact of debris on marine life. *Mar. Pollut. Bull.* 92, 170–179.
- Garaba, S., Dierssen, H., 2018. An airborne remote sensing case study of synthetic hydrocarbon detection using short wave infrared absorption features identified from marine-harvested macro- and microplastics. *Remote Sens. Environ.* 205, 224–235.
- Gregory, M., Andrady, A., 2003. Plastics in the marine environment. In: *Andrady, A. (Ed.), Plastics and the Environment*. John Wiley, New Jersey, pp. 379–401.
- Hardesty, B., Good, T., Wilcox, C., 2015. Novel methods, new results and science-based solutions to tackle marine debris impacts on wildlife. *Ocean Coast. Manag.* 115, 4–9.
- Hasituya, Z., Chen, L., Wu, W., Jiang, Z., Li, H., 2016. Monitoring plastic-mulched farmland by Landsat-8 OLI imagery using spectral and textural features. *Remote Sens.* 8 (4), 353.
- Hidalgo-Ruz, V., Thiel, M., 2013. Distribution and abundance of small plastic debris on beaches in the SE Pacific (Chile): a study supported by a citizen science project. *Mar. Environ. Res.* 87–88, 12–18.
- Hinojosa, I., Thiel, M., 2009. Floating marine debris in fjords, gulfs and channels of southern Chile. *Mar. Pollut. Bull.* 58, 341–350.
- Hinojosa, A., Rivadeneira, M., Thiel, M., 2011. Temporal and spatial distribution of floating objects in coastal waters of central-southern Chile and Patagonian fjords. *Cont. Shelf Res.* 31, 172–186.
- Hörig, B., Kühn, F., Oschütz, F., Lehmann, F., 2010. HyMap hyperspectral remote sensing to detect hydrocarbons. *Int. J. Remote Sens.* 22 (8), 1413–1422.
- Huang, C., Davis, L.S., Townshen, J.R.G., 2002. An assessment of support vector machines for land cover classification. *Int. J. Remote Sens.* 23 (4), 725–749.
- Huntington, J., Whitbourn, L., Mason, P., Berman, M., Schodlok, M.C., 2010. HyLogging - voluminous industrial-scale reflectance spectroscopy of the earth's subsurface. In: *Proc. ASD IEEE GRS. Art. Sci. Appl. Reflectance Spectrosc. Symp., Boulder, CO Vol. II*. pp. 1–14 (14pp).
- Hyrenbach, D., Kennish, J., 2008. Question 6: how does marine debris affect wildlife and the environment? In: *Williams, M., Ammann, E. (Eds.), Marine Debris in Alaska*:

- Coordinating our Efforts. Alaska Sea Grant College Program, University of Alaska Fairbanks, pp. 109–120.
- ICC (International Coastal Cleanup), 2009. A Rising Tide of Ocean Debris: And What We can Do about it. Ocean Conservancy (64p).
- Immitzer, M., Atzberger, C., Koukal, T., 2012. Tree species classification with random forest using very high spatial resolution 8-band worldView-2 satellite data. *Remote Sens.* 4 (9), 2661–2693.
- Ivar do Sul, J., Costa, M., 2007. Marine debris review for Latin America and the wider Caribbean region: from the 1970s until now, and where do we go from here? *Mar. Pollut. Bull.* 54, 1087–1104.
- Jara, C., Jaramillo, E., 1979. Hallazgo de *Planes marinus* Rathbun, 1914, sobre boya a la deriva en bahía de Maquillahue Chile (Crustácea. Decapoda, Grapsidae). In: Medio ambiente. 4. pp. 108–113.
- Kiessling, T., Salas, S., Mutafoğlu, K., Thiel, M., 2017. Who cares about dirty beaches? Evaluating environmental awareness and action on coastal litter in Chile. *Ocean Coast. Manag.* 137, 82–95.
- Kuhn, M., Johnson, K., 2013. *Applied Predictive Modeling*, 2nd ed. Springer, New York, NY, USA.
- Kühn, F., Oppermann, K., Hörig, B., 2004. Hydrocarbon index—an algorithm for hyper-spectral detection of hydrocarbons. *Int. J. Remote Sens.* 25 (12), 2467–2473.
- Lavender, K., 2017. Plastics in the marine environment. *Annu. Rev. Mar. Sci.* 9, 205–229.
- Lee, J., Hong, S., Song, Y., Hong, S., Jang, Y., Jang, M., Heo, N., Han, G., Lee, M., Kang, D., Shim, W., 2013. Relationships among the abundances of plastic debris in different sizeclasses on beaches in South Korea. *Mar. Pollut. Bull.* 77, 349–354.
- Matasci, G., Longbotham, N., Pacifici, F., Kanevski, M., Tuia, D., 2015. Understanding angular effects in VHR imagery and their significance for urban land-cover model portability: a study of two multi-angle in-track image sequences. *ISPRS J. Photogramm. Remote Sens.* 107, 99–111.
- Matthew, M., Adler-Golden, S., Berk, A., Richtsmeier, S., Levine, R., Bernstein, L., Acharya, P., Anderson, G., Felde, G., Hoke, M., Ratkowski, A., Burke, H., Kaiser, R., Miller, D., 2000. Status of Atmospheric Correction Using a MODTRAN4-based Algorithm. In: *SPIE Proceedings, Algorithms for Multispectral, Hyperspectral, and Ultraspectral Imagery VI 4049*, pp. 199–207.
- McElwee, K., Donohue, M., Courtney, C., Morishige, C., Rivera-Vicente, A., 2012. A strategy for detecting derelict fishing gear at sea. *Mar. Pollut. Bull.* 65 (1–3), 7–15.
- Michez, A., Piégay, H., Jonathan, L., Claessens, H., Lejeune, P., 2016. Mapping of riparian invasive species with supervised classification of Unmanned Aerial System (UAS) imagery. *Int. J. Appl. Earth Obs. Geoinf.* 44, 88–94.
- Morishige, C., McElwee, K., 2012. At-sea detection of derelict fishing gear in the North Pacific: an overview. *Mar. Pollut. Bull.* 65, 1–6.
- Mouat, J., Lopez, R., Bateson, H., 2009. *Economic Impacts of Marine Litter*. KIMO International, Escocia.
- Nelms, S., Coombes, C., Foster, L., Galloway, T., Godley, B., Lindeque, P., Witt, M., 2017. Marine anthropogenic litter on British beaches: a 10-year nationwide assessment using citizen science data. *Sci. Total Environ.* 579, 1399–1409.
- Newman, S., Watkins, E., Farmer, A., Brink, P., Schwitzer, J., 2015. The economics of marine litter. In: Bergmann, M. (Ed.), *Marine Anthropogenic Litter*, pp. 367–394.
- Novelli, A., Tarantino, E., 2015. Combining ad hoc spectral indices based on LANDSAT-8 OLI/TIRS sensor data for the detection of plastic cover vineyard. *Remote Sens. Lett.* 6 (12) (993–941).
- Pacifici, F., 2013. An automatic atmospheric compensation algorithm for very high spatial resolution imagery and its comparison to FLAASH and QUAC. In: *Proceedings JACIE*, pp. 1–43.
- Pacifici, F., 2016. Validation of the DigitalGlobe surface reflectance product. In: *International Geoscience and Remote Sensing Symposium (IGARSS)*, pp. 1973–1975.
- Pacifici, F., Longbotham, N., Emery, W.J., 2014. The importance of physical quantities for the analysis of multitemporal and multiangular optical very high spatial resolution images. *IEEE Trans. Geosci. Remote Sens.* 52, 6241–6256.
- Pal, M., 2005. Random forest classifier for remote sensing classification. *Int. J. Remote Sens.* 26 (1), 217–222.
- Pesce, O.H., Moreno, P.I., 2014. Vegetation, fire and climate change in central-east Isla Grande de Chiloé (43°S) since the Last Glacial Maximum, northwestern Patagonia. *Quat. Sci. Rev.* 90, 143–157.
- Pham, C., Ramirez-Llodra, E., Alt, C., Amaro, T., Bergmann, M., Canals, M., et al., 2014. Marine litter distribution and density in European seas, from the shelves to deep basins. *PLoS One* 9 (4), e95839. <https://doi.org/10.1371/journal.pone.0095839>.
- Pichel, W., Veenstra, T., Churnside, J., Arabini, E., Friedman, K., Foley, D., et al., 2012. GhostNet marine debris survey in the Gulf of Alaska – Satellite guidance and aircraft observations. *Mar. Pollut. Bull.* 65, 28–41.
- PlasticsEurope, 2012. *Plastics – The Facts 2012: An Analysis of European Plastics Production, Demand and Waste Data for 2011*.
- PlasticsEurope, 2015. *Plastics – The Facts 2015 – PlasticsEurope*, Belgica.
- Price, J.C., 1994. How Unique Are Spectral Signatures? *Remote Sens. Environ.* 49, 181–186.
- Puissant, A., Rougier, S., Stumpf, A., 2014. Object-oriented mapping of urban trees using Random Forest classifiers. *Int. J. Appl. Earth Obs. Geoinf.* 26, 235–245.
- Rochman, C., Browne, M., 2013. Classify plastic waste as hazardous. *Nature* 494, 169–170.
- Rodríguez-Galiano, V.F., Ghimire, B., Rogan, J., Chica-Olmo, M., Rigol-Sánchez, J.P., 2012. An assessment of the effectiveness of a random forest classifier for land-cover classification. *ISPRS J. Photogramm. Remote Sens.* 67 (1), 93–104.
- Romera-Castillo, C., Pinto, M., Langer, T., Álvarez-Salgado, X., Herndl, G., 2018. Dissolved organic carbon leaching from plastics stimulates microbial activity in the ocean. *Nat. Commun.* 9, 1430.
- Schodlok, M.C., Whitbourn, L., Huntington, J., Mason, P., Green, A., Berman, M., Coward, D., Connor, P., Wright, W., Jolivet, M., Martínez, R., 2016. HyLogger-3, a visible to shortwave and thermal infrared reflectance spectrometer system for drill core logging: functional description. *Aust. J. Earth Sci.* 99, 1–12.
- Sepúlveda, H.H., Artañ, O.E., Torregrosa, C., 2011. LiveROMS: a virtual environment for ocean numerical simulations. *Environ. Model. Softw.* 26 (11), 1372–1373.
- SERNAPESCA (Servicio Nacional de Pesca y Acuicultura), 2015. *Anuario 2015 – Cosechas CC Región*. http://www.sernapesca.cl/index.php?option=com_remository&Itemid=246&func=fileinfo&id=22583, Accessed date: 23 February 2017.
- Slonicker, G., Fisher, B., Aiello, D.P., Haack, B., 2010. Visible and infrared remote imaging of hazardous waste: a review. *Remote Sens.* 2 (11), 2474–2508.
- Thiel, M., Hinojosa, I., Vásquez, N., Macaya, E., 2003. Floating marine debris in coastal waters of the SE-Pacific (Chile). *Mar. Pollut. Bull.* 46 (2), 224–231.
- Thompson, R.C., Moore, C.J., Vom Saal, F.S., Swan, S.H., 2009. Plastics, the environment and human health: current consensus and future trends. *Philos. Trans. R. Soc. B* 364 (1526), 2153–2166.
- Thuiller, W., Lafourcade, B., Engler, R., Araújo, M.B., 2009. BIOMOD – a platform for ensemble forecasting of species distributions. *Ecography* 32, 369–373.
- UNEP (United Nations Environment Programme), IOC (Intergovernmental Oceanographic Commission), 2009. *UNEP/IOC guidelines on survey and monitoring of marine litter*. In: *Regional Seas Reports and Studies No 186. IOC Technical Series No 83*. Nairobi (131p).
- Unger, B., Rebolledo, E., Deaville, R., Gröne, A., IJsseldijk, L., Leopold, M., et al., 2016. Large amounts of marine debris found in sperm whales stranded along the North Sea coast in early 2016. *Mar. Pollut. Bull.* 112, 134–141.
- Watters, D., Yoklavich, M., Love, M., Schroeder, D., 2010. Assessing marine debris in deep seafloor habitats off California. *Mar. Pollut. Bull.* 60, 131–138.
- Woodall, L.C., Sanchez-Vidal, A., Canals, M., Paterson, G.L.J., Coppock, R., Sleight, V., Calafat, A., Rogers, A.D., Narayanaswamy, B.E., Thompson, R.C., 2014. The deep sea is a major sink for microplastic debris. *R. Soc. Open Sci.* 1.
- Zhong, Y., Zhang, L., 2012. An adaptive artificial immune network for supervised classification of multi-/hyperspectral remote sensing imagery. *IEEE Trans. Geosci. Remote Sens.* 50 (3), 894–909.